NANO · MICRO small
www.small-journal.com

A Counter Propagating Lens-Mirror System for Ultrahigh Throughput Single Droplet Detection

Xiaobao Cao, Ying Du, Andreas Küffner, Jordan Van Wyk, Paolo Arosio, Jing Wang, Peter Fischer, Stavros Stavrakis, and Andrew deMello**

Fluorescence-based detection schemes provide for multiparameter analysis in a broad range of applications in the chemical and biological sciences. Toward the realization of fully portable analysis systems, microfluidic devices integrating diverse functional components have been implemented in a range of out-of-lab environments. That said, there still exits an unmet and recognized need for miniaturized, low-cost, and sensitive optical detection systems, which provide not only for efficient molecular excitation, but also enhanced photon collection capabilities. To this end, an optofluidic platform that is adept at enhancing fluorescence light collection from microfluidic channels is presented. The central component of the detection module is a monolithic parabolic mirror located directly above the microfluidic channel, which acts to enhance the number of emitted photons reflected toward the detector. In addition, two-photon polymerization is used to print a microscale-lens below the microfluidic flow channel and directly opposite the mirror, to enhance the delivery of excitation radiation into the channel. Using such an approach, it is demonstrated that fluorescence signals can be enhanced by over two orders of magnitude, with component parallelization enabling the detection of pL-volume droplets at rates up to 40 000 droplets per second.

1. Introduction

Since their introduction, droplet-based microfluidic systems have become one of the most important components of the microfluidic technology set, due to their unique features and wide range of potential applications.[1,2] In simple terms, droplet-based microfluidic systems leverage the essential advantages of all microscale systems (such as reduced sample volumes and outstanding control of heat and mass transport) whilst overcoming issues (such as Taylor dispersion, inefficient mixing, and unwanted surface–molecule interactions) that beset single-phase microfluidic systems.[3] Additionally, droplet-based microfluidic systems enable the ultrafast formation of sub-nL assay volumes, where droplet payloads may be controlled in a rapid and efficient manner. All these features, ensure that droplets are ideally suited for ultra-high-throughput chemical and biological experimentation in areas such as single molecule analysis,[4] DNA amplification,[5] protein crystallization,[6] high-throughput screening,[7,8] and single-cell analysis.[9]

One of the most important challenges faced when using droplet-based microfluidic systems is the ability to analyze droplet contents in a rapid and quantitative fashion. Indeed, it could be argued that the development of appropriate analytical detection techniques remains the most critical aspect defining the utility and potential application of microfluidic systems in general. In this regard, the exploitation of optical microstructures provides new opportunities for signal enhancement when sensing droplet contents in a high-throughput manner. Fluorescence imaging is commonly used to detect and visualize fluorescence

Dr. X. B. Cao, Dr. Y. Du, A. Küffner, Prof. P. Arosio, Dr. S. Stavrakis, Prof. A. deMello
Institute for Chemical and Bioengineering
ETH Zürich
Vladimir-Prelog-Weg 1, Zurich 8093, Switzerland
E-mail: stavros.stavrakis@chem.ethz.ch; andrew.demello@chem.ethz.ch
Dr. X. B. Cao
School of Mechatronical Engineering
Beijing Institute of Technology
5 South Zhongguancun Street, Beijing 100081, China
Dr. Y. Du
College of Sciences
Zhejiang University of Technology
Hangzhou 310023, China
J. V. Wyk
Nanotechnology Engineering
University of Waterloo
200 University Avenue West, Waterloo, Ontario N2L 3G1, Canada
Prof. J. Wang
Institute of Environmental Engineering
ETH Zurich
Vladimir-Prelog-Weg 1, Zurich 8093, Switzerland
Prof. P. Fischer
IFNH Food Process Engineering Group
ETH Zurich
Schmelzbergstrasse 7, Zürich 8092, Switzerland
The ORCID identification number(s) for the author(s) of this article can be found under https://doi.org/10.1002/smll.201907534.

DOI: 10.1002/smll.201907534

from micron-scale objects, such as cells[10,11] and particles.[12,13] Although fluorescence is a robust, nondestructive and highly sensitive tool to assay droplet contents, droplet volumes are typically on the order of a few picoliters, and thus emission signals are normally low. That said, the efficient analysis of pL volumes is far from simple, especially when molecular concentrations are in the nanomolar or sub-nM range. Indeed, in such situations, confocal set-ups and cooled photomultiplier tubes (PMTs) are normally required to ensure requisite detection limits. Although efficient, such an approach is costly and hinders facile parallelization for high-throughput analysis. To address such limitations, much recent effort has been focused on realizing efficient schemes for droplet detection. For example, integrated comprehensive droplet digital detection (IC-3D) has been shown to allow for the analysis of droplet-encapsulated bacteria at rates in excess of 10^5 droplets per second, through use of a rotating cuvette.[14] More recently a cell phone-based optofluidic platform realized the generation and detection of droplets at rates of 10^6 droplets per second.[15] In addition, Yelleswarapu et al. reported an optofluidic platform that miniaturizes and integrates digital (ELISA-based) assays, demonstrating the detection of droplets at a throughput of $\approx 10^5$ droplets per second, using time domain-encoded fluorescence detection.[16] However, despite its undoubted utility, such an approach necessitates the use of low flow rates and complex digital processing algorithms, and thus is not of wide applicability. Additionally Tang and colleagues have presented the use of a CMOS senor array to detect fluorescent droplets at rates approaching 250 000 droplets per second,[17] with Schonbrun et al. demonstrating the fluorescence imaging of ≈200 000 droplets per second using a microfabricated zone-plate array integrated into a parallelized microfluidic device.[18] Significantly, however, no quantitative assessment of either methods has been reported. Finally, Easley and co-workers recently described a continuous referencing scheme (incorporating automated optical modulation with lock-in detection) for droplet analysis that yields picomolar detection limits, albeit at very low-throughput.[19]

Although microscopes provide for high spatial resolution imaging and high collection efficiencies (due to the use of lenses with high numerical apertures), their fields of view (FOV) are normally restricted. These issues prevent high-speed imaging of micron-sized objects moving at high velocities and over large areas; a task that is central to flow cytometry and high-throughput screening. As noted, conventional objectives possess excellent light gathering abilities, but because of their high magnifications have restricted fields of view. Conversely, low magnification objectives have large FOVs, but reduced photon collection efficiencies (due to their low numerical apertures). Unsurprisingly, much recent activity has focused on the monolithic integration of functional optical components within chip-based microfluidic systems.[20–24] Most of these "on-chip" optical components have been used to ensure the effective delivery of excitation light to a sample, with sensitive microscopes or imagers being used to detect emission signals.[18,25,26] There is however, a recognized and pressing need to develop integrated, sensitive and low-cost detection systems, which provide not only efficient sample excitation, but also enhanced fluorescence collection capabilities. To this end, integrated microlenses have been used to enhance signal intensities and mimic the optical performance of conventional objective lenses.[27,28] Additionally, microlens arrays have been shown to be adept in simultaneously imaging micron-scale objects spread over large areas, thus providing access to large FOVs.[22] For example, Schonbrun et al. demonstrated image-based screening of large collections of cells at moderate throughputs (2275 cells per second) within a microfabricated device, by combining bright field microscopy and microlens arrays.[29]

Microlenses can be fabricated using a variety of techniques, including photoresist reflow and transfer,[30] hot embossing[31] micromolding,[32] and soft lithography.[33] Since microlenses provide for enhanced signal intensities, they are especially useful when performing high-speed imaging of rapidly moving objects. For example, Baret and co-workers recently reported an 8-times signal enhancement when probing segmented flows by aligning a microlens array on top of a silver-coated microchannel.[22] In addition, Fan et al. presented an embedded microball lens array for high-throughput multi-color fluorescence detection of micron-sized particles and cells.[34] As noted, and although fluorescence techniques provide for high analytical sensitivities and low background noise, it is still a significant challenge to detect reduced amounts of analyte within pL-volume droplets. Consideration of all these factors highlights the importance of developing new modalities that allow detection in small volumes and at low analyte concentrations. To this end, we present an integrated, high-throughput optofluidic platform for fluorescence-based droplet detection. To provide for high sensitivity analysis, microlens-micromirror units are embedded within a droplet-based microfluidic platform in a co-axial geometry. Such a lens-mirror combination can be used to effectively increase the local numerical aperture, and combines the advantages of low magnification objectives in providing large fields of view, with the high collection efficiencies of high numerical aperture objectives.

2. Results and Discussion

2.1. Optofluidic Device

The developed optofluidic system is schematically presented in **Figure 1**a. A partially enlarged view of the microfluidic channel array is shown in Figure 1b, with the array of microlenses being aligned with the micromirror array on the opposite substrate layer (Figure 1c). A representative microlens is shown in Figure 1d and is designed to generate an optical focus at the center plane of the underlying microchannel. The SEM image demonstrates the exquisite control of lens dimensions, but also reveals a degree of surface roughness; a result of the layer-by-layer 3D printing process used in fabrication. It should be noted that the surface could be further smoothed through variation of the photoresist chemistry and printer parameters (such as the slicing distance, hatching distance, laser power, printing speed and developing time[35–37]). As illustrated in Figure 1e, the entire module comprises of a parabolic mirror placed above the microfluidic channel and a microlens located below the microfluidic channel. The parabolic mirror acts as a circular reflector to increase the amount of light directed back into the objective, with the lens being used to both focus the excitation light into

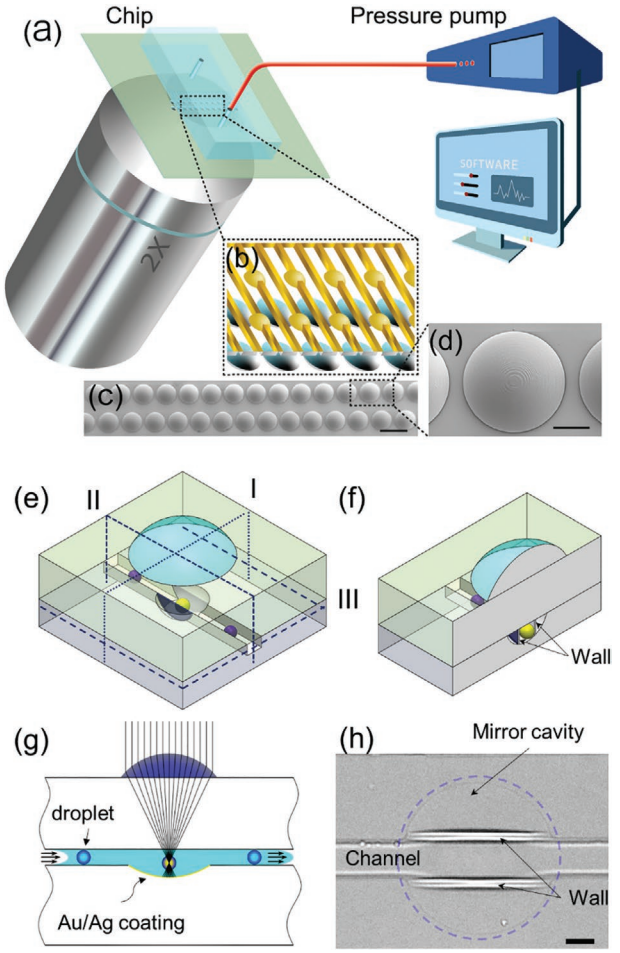

Figure 1. a) Schematic of the lens-mirror system. b) Schematic showing parallel mirrors vertically aligned with the center of a channel. c) SEM image of two rows of microlenses. d) SEM image of a single focusing microlens. e) Overview of the lens mirror system, with dashed lines (I), (II), and (III) representing the different cross section. f,g) Vertical cross sections through the microfluidic device. h) Transverse cross section image through the microfluidic channel showing the wall layer, scale bar: 50 µm.

the microchannel and collect emitted photons. The surface of the mirror was coated with a reflective a 100 nm thick gold film and a 150 nm thick silver overcoat to yield a reflection efficiency in excess of 90%. However, the presence of the curved microchannel surface, (which serves as the parabolic mirror) causes a slight displacement in droplet motion (in the lateral direction) away from the focusing region, which acts to reduce both excitation and collection efficiencies. To circumvent this problem, two additional photoresist layers parallel to the channel walls (shown in Figure 1f,h) were embedded within the mirror cavity to guide droplets in the lateral direction.

COMSOL simulations were used to assess both the focal length and light collection capabilities of the microlens-mirror pair at 532 nm. The focal length of a microlens is defined as the distance between the focusing plane of collimated light and the interface of the microlens and glass coverslip, as shown in **Figure 2**a. Importantly, the photoresist used to fabricate the microlens absorbs minimally in the visible region of the electromagnetic spectrum (Figure S1, Supporting Information) and exhibits negligible autofluorescence. A lens with a diameter (d) of 160 µm and height (h) of 50 µm were used in all simulations, with the real parts of the refractive index estimated to be 1.60 and 1.51 for the microlens and the glass coverslip, respectively. The parabolic focusing reflector has a height of 35 µm, a width of 120 µm and a profile described by $y = -x^2/80$ (Figure 2b). Ray-tracing simulations indicate that incident radiation is focused at a distance of 175 µm from the glass-microlens interface, and in the center of the channel, with emission from a point source radiating in all directions (4π steradians). Significantly, simulations predict that ≈73.9% of the incident radiation is reflected back toward the microlens.

To demonstrate operation of this optical geometry at high analytical throughput, an integrated microfluidic device comprising 80 microchannels bearing with silver coated curved shaped regions aligned within an embedded high numerical aperture refractive microlens array was fabricated, allowing for high sensitivity detection over a 6.4 × 0.32 mm field of view.

2.2. Characterization of the Counter Propagating Lens-Mirror System

Figure 3a–c presents images of a droplet (containing 100 × 10^{-6} M FITC) moving along bare, metal-coated and microlens-mirror pair-integrated microfluidic channels, respectively. Figure 3d–f shows the corresponding emission intensity profiles extracted from the dashed lines in Figure 3a–c. Contrast (luminance difference) was adjusted in all images to ensure that fluorescence droplets in the bare microchannel (Figure 3a) are clearly visible, and necessarily means that droplets moving along microchannel integrating mirror-lens structures are overexposed (Figure 3c). As can be clearly seen, introduction of the metal coating enhances analytical signals by approximately threefold (Figure 3d,e) due to the fact that a significant portion of the emission light is directed back toward the microscope objective. Such amplification is further enhanced by the presence of the microlens-coated mirror pair. To quantify the signal enhancement, average fluorescence intensities were measured over an area of 5 × 5 pixels under each microlens-mirror pair. To this end, Figure 3g presents a fluorescence intensity time trace during which droplets containing a 150 × 10^{-6} M FITC solution are motivated along a microchannel. Individual droplets at each single microlens-mirror pair (moving at a velocity of 4.3 mm s^{-1}) pass through the focused light spot with emission photons being recorded over an exposure time of 300 µs at 3000 frames per second. Significantly, data show that each droplet produces a strong photon burst as it passes through the focal volume of a single microlens-mirror structure, giving rise to a signal enhancement of 117-fold (over two orders of magnitude compared to signals obtained in bare microfluidic channels). To assess whether each lens-mirror pair generates the same collection efficiency, coefficients of variation (CVs) of fluorescence intensity (analyzed from corresponding peak height histograms) for 4 different lenses, were calculated as: 5.14%, 5.30%, 5.92%, and 6.18% (Figure S2, Supporting Information). The similarity in these values demonstrates the consistency in the two-photon lithography printing process, affording

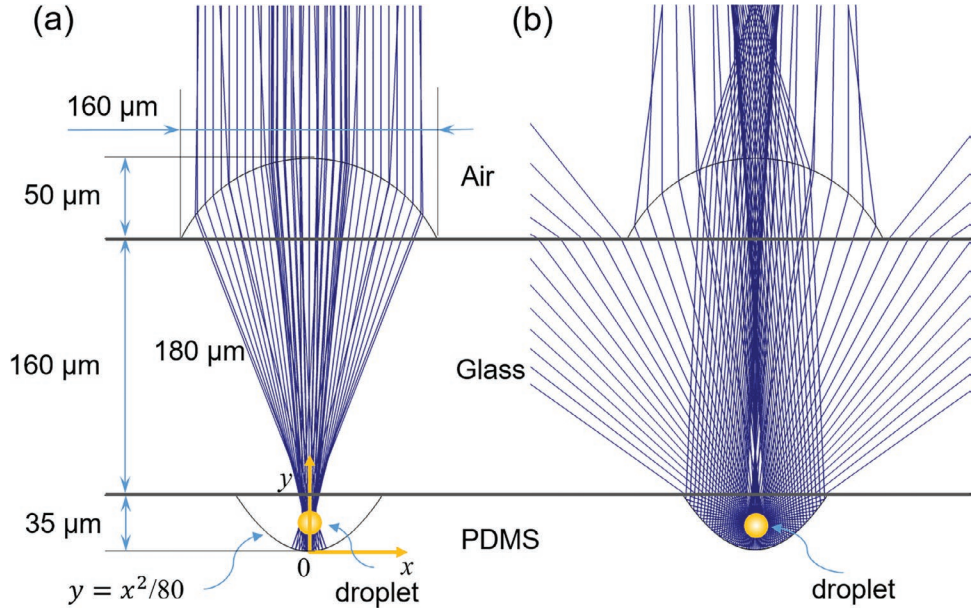

Figure 2. Results of COMSOL Multiphysics ray-tracing simulations, highlighting ray trajectories through the optofluidic device, package a) Simulation of excitation light through the vertical cross-section. b) Simulation of the emission light produced within a droplet volume through the vertical cross-section.

precise alignment between each microlens and micromirror. It is important to note that the current device operates optimally for certain droplet volumes. Based on the diameter of the excitation beam spot (between 5 and 10 µm), all droplets with a volume in excess of 65 fL will be detected. Indeed, and provided that the droplet content is homogenous, efficient detection of much larger nL volume droplets is possible.

To assess the concentration detection limit of the system, average fluorescence intensities were measured as a function of fluorescein concentration between 100×10^{-9} and 10×10^{-6} M (Figure 3h), with each data point corresponding to a mean fluorescence intensity of 200 droplets (error bar: one standard deviation). As can be observed, signals exhibit a linear dependence on molecular concentration over the entire range, with a limit of detection of 50×10^{-9} M. Indeed, Figure 3i demonstrates that fluorescence signals can be clearly discriminated from background when probing droplets containing 100×10^{-9} M fluorescein, with a signal to noise ratio of 12.4. It should also be noted that accessible detection limits could be further decreased by adoption of a higher power excitation source and a higher quantum efficiency camera. Moreover, an increase in the exposure time will lead to further improvements without any loss in information content.[22]

The variability of the fluorescence signal amongst different detection geometries was evaluated by calculating the coefficient of variation as the ratio of the standard deviation to the mean. Figure 3j,k presents fluorescence intensity histograms for droplet populations (n = 5000) in the absence and presence of the counter propagating microlens-mirror pair, with exposure times of 20 ms and 200 µs, respectively. The CV of fluorescence intensities detected in conventional static measurements under a fluorescence microscope was ≈6.37% (Figure 3j) for a 20 ms exposure time. Significantly, this is similar to that obtained from the microlens-mirror pair optofluidic system, which yields a 7.56% CV for a 0.2 ms exposure time (Figure 3k). The similarity in CV demonstrates that the microlens-mirror pair signal enhancement affords both sensitive and quantitative detection of droplet contents at high-throughput. Indeed, despite the fact that there is a difference of over two orders of magnitude in exposure times between the two optical approaches, both generate similar CVs.

Finally, to assess the capability of the system to detect droplets at extremely high rates, droplets (produced at a flow focusing geometry shown in Figure S3, Supporting Information) were injected into the device through an array of parallel channels at a pressure of 200 mBar. The use of low magnification objectives offers the advantage of an increased FOV that can encompass many parallel microfluidic channels, as shown in Figure 1c. When imaging with a 2 × objective, the FOV covers 80 microlens-mirror units with an imaging region of 2048 × 8 pixels (with a pixel size of 6.5 µm), corresponding to an area of 6656 µm × 26 µm. With a camera frame rate of 8500 fps and an exposure time of 30 µs, 28269 droplets were detected in 706 ms, corresponding to an analytical throughput of 40 000 droplets per second (Movie S1, Supporting Information).

2.3. Detection of Adenylate Kinase in Single Cells

Detection of protein expression at the single cell level and at high-throughput requires methods that are both sensitive and fast. To demonstrate the potential utility of our optofluidic system in this regard, we assayed heterogeneity in the expression of adenylate kinase in *Escherichia coli* cells. Specifically, a bacterial suspension was co-encapsulated in droplets at the single-cell level with a reagent mix (containing the adenylate kinase activity assay kit and a lysis buffer) using a flow focusing droplet generator. As noted, the assay measures adenylate

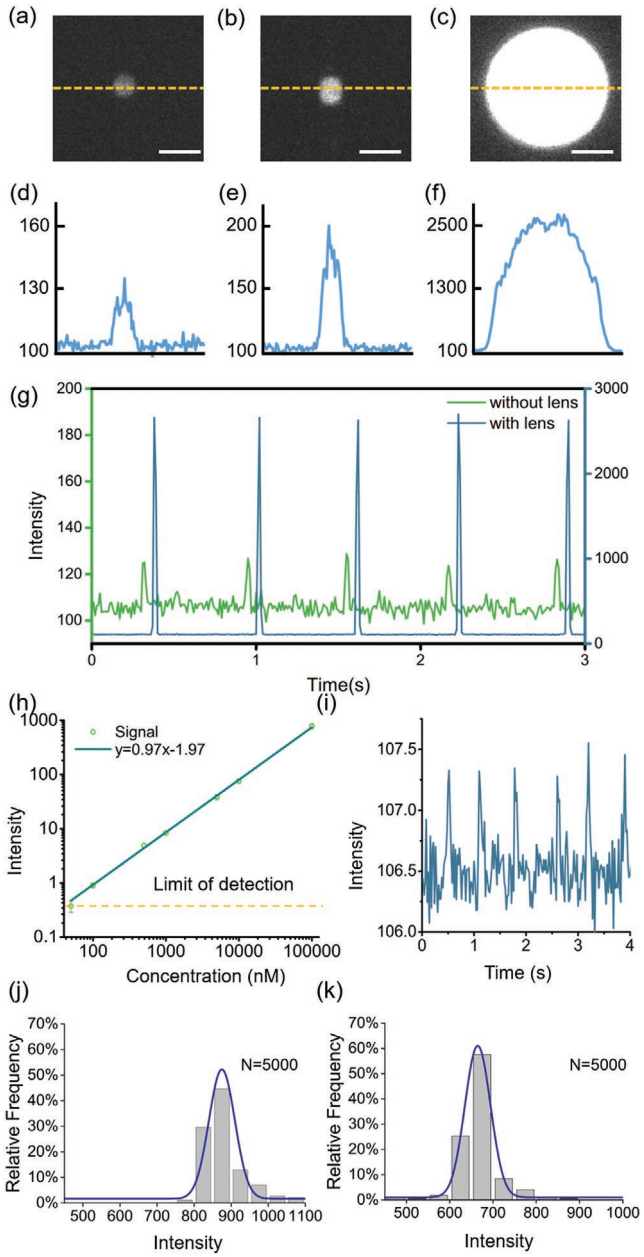

Figure 3. Characterization of microlens-mirror pairs. Images in a–c) show fluorescent droplets within an empty channel, a metal coated channel and a channel containing a mirror-lens structure respectively. Scale bars are 100 µm. Plots in d–f) show emission density profiles along the corresponding yellow dashed lines in (a–c), respectively. g) Fluorescence time trace reporting the signal enhancement when using the lens-mirror array. The blue curve shows signals from FITC droplet when using the lens-mirror system, and the green curve shows FITC droplet signals without lens system. h) Linear dependence of fluorescence signal as a function of fluorescein concentration for 11 pL volume droplets flowing through the microlens-mirror pairs. Each data point represents the mean fluorescence signal of 200 droplets and the associated standard error in the mean. i) Raw signal for droplets containing fluorescein at a concentration of 100×10^{-9} M. j) Relative intensity distribution of static droplets containing 100×10^{-6} M FITC detected using a 2x NA 0.05 objective. k) Relative intensity distribution of flowing droplets containing 100×10^{-6} M FITC passing through the microlens-mirror pair structure.

kinase activity by detecting adenosine triphosphate (ATP) generated from adenosine diphosphate (ADP) as a substrate. ATP is detected via a multi-step reaction, resulting in the generation of an intermediate that reacts with an adenylate kinase probe forming a fluorescence product that emits at 587 nm. To ensure single-cell occupancy, the bacterial sample was segmented under limiting dilution conditions following Poisson statistics, such that each drop contains either one cell or no cell. Under such conditions, ≈15% of all droplets contain a single cell, with less than 2% having two or more cells. Furthermore, extraction of the enzyme from bacterial cells allows the detection of the fluorescence product within the droplet content (**Figure 4**a), and ensures minimal product dilution. All droplets were analyzed using the counter propagating microlens-mirror detection array with the intensity distribution of the droplet population being shown in Figure 4b. The red peak in Figure 4b reports the distribution of droplets containing kinase proteins extracted from single *E. coli* cells within each droplet, with the blue peak reporting the population of the empty droplets carrying only the reagent mix. A total of 47 043 droplets were measured over a period of 1.5 s, with 7226 and 39 817 droplets representing single cell and background events, respectively. Approximately, 18.1% of the droplet population shows a fluorescent signal representative of a single cell event; a value that is consistent with the prediction based on Poisson statistics. These results clearly demonstrate that the microlens-mirror optofluidic platform can be used for sensitive and ultra-high-throughput analysis of single cell experiments, with the presented data confirming a broad distribution of kinase expression in single cells, as result of "noisy" transcription (Figure 4b inset).

3. Conclusions

We have demonstrated that the integration of microfabricated optical components within a microfluidic system can be used to generate an optofluidic platform adept at high-sensitivity and high-throughput droplet and single cell analysis. The counter propagating microlens-mirror system employs a monolithic lens to effectively deliver excitation light into the microfluidic channel, with the parabolic mirror collecting up to 80% of the emitted fluorescence light. Such an arrangement significantly improves the efficiency of excitation light delivery and fluorescence collection leading to a 120-fold signal enhancement compared to the plain microfluidic channel. To explore the high-throughput capabilities of this optical geometry, 80 parallel microlens-mirror pairs embedded in a microfluidic platform were used to detect adenylate kinase at the single cell level, achieving an analytical throughput of 40 000 droplets per second. Such performance allows for ultra-high-throughput single cell experiments, whilst obviating the need for expensive high NA objectives and providing a cost-effective route to a range of high-throughput experiments within pL-volume droplets. The modular design of the device is applicable to many other functional single cell assays, where statistical information from large populations of individual cells must be collected while each cell is contained within an isolated microenvironment. Moreover, we expect that our optofluidic systems could form the basis of a fully integrated detection platform readily

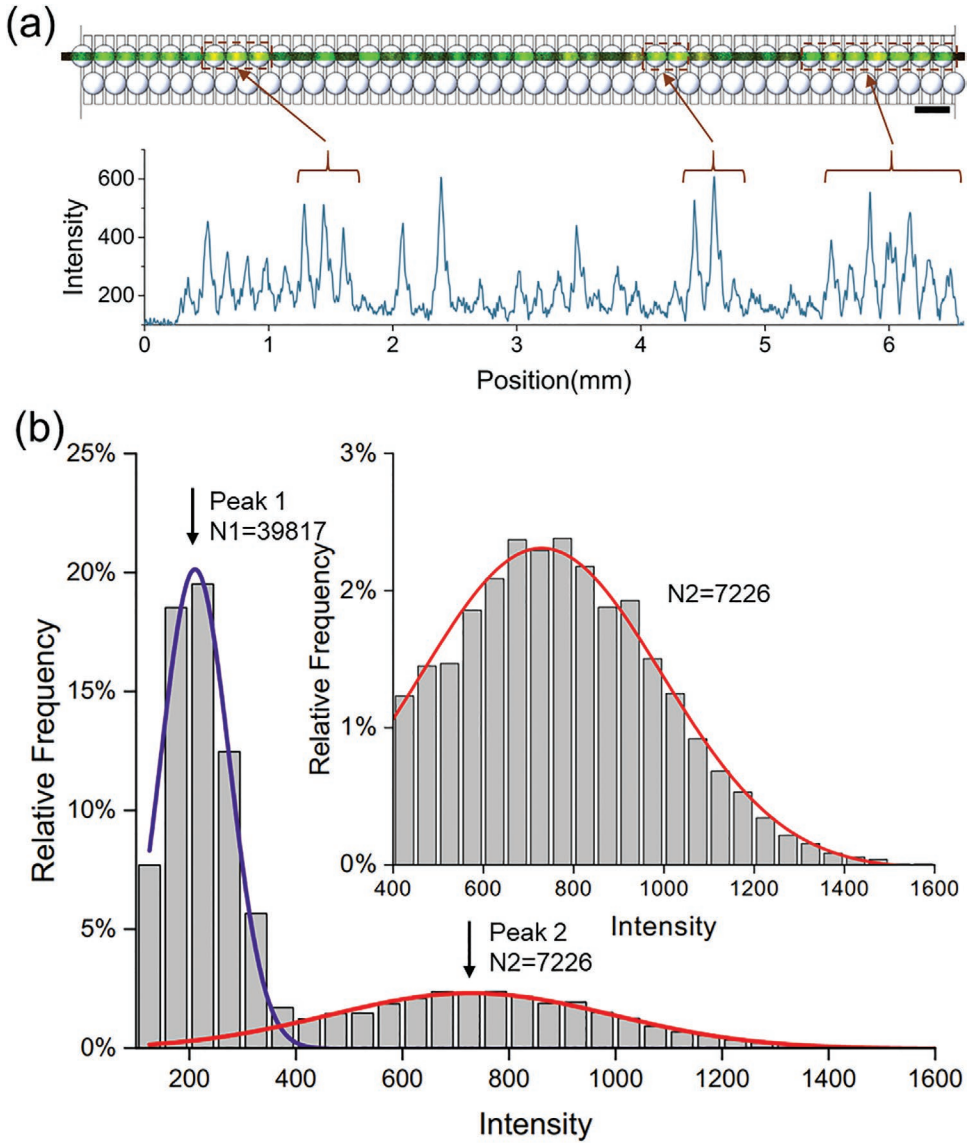

Figure 4. a) Snapshot of fluorescent droplets passing through a parallel microlens-mirror pair array (top; scale bar = 500 µm). Intensity profile of single droplets along one row of the microlens-mirror array (bottom). Arrows indicate the positions of representative peaks. b) Fluorescence intensity distribution of droplet intensities obtained in the single-cell activity assay ($N = 47043$). Of these, 39 817 droplets were empty (peak 1, blue), whilst 7226 contain a single bacterium (peak 2, red). Inset: Enlarged view of the histogram for droplets containing single cells. The red and blue curves represent Gaussian fits to the data.

accessible to many end-user research laboratories with requirements in the single cell analysis/flow cytometry space.

4. Experimental Section

Reagents: DNA sequences encoding Adenylate Kinase from *E. Coli* and Green Fluorescent Protein were synthesized, codon optimized for expression in *E. coli*, and cloned into the pET-15b vector (by Genewiz, New Jersey, USA). An *E. coli* strain (BL21-GOLD (DE3)) was used as an expression system for recombinant proteins. The amino acid sequences of the recombinant proteins employed in this study are listed in Table S1 (Supporting Information). Cells were transformed by heat shock and transformed colonies were selected on LB agar plates with 100 µg mL^{-1} ampicillin. Thereafter, cells were pre-cultured in 50 mL of LB medium mixed with 100 µg mL^{-1} of ampicillin for 12 h. The pre-culture was subsequently used to seed 4 cultures of 0.5 L LB medium with 100 µg mL^{-1} ampicillin. Cultures were incubated for 4 h at 37 °C until the optical density at 600 nm was 0.7. Afterward, recombinant expression was induced using 0.5×10^{-3} M isopropyl D-thiogalactopyranoside (99%, PanReac AppliChem) and cultures incubated for an additional 16 h at 20 °C. The fresh cell suspension with the respective overexpressed protein was directly used in subsequent experiments. Bacterial cultures were centrifuged at 4500 rpm for 15 min and the resulting pellet resuspended in PBS (phosphate buffered saline) buffer (Sigma-Aldrich, Buchs, Switzerland). For microtiter plate experiments, bacterial suspensions were diluted until the optical density at 600 nm was 0.01. For microfluidic experiments, bacterial suspensions were also diluted in PBS until the optical density at 600 nm was 0.01, and then transferred into a glass reservoir. Green fluorescent protein (GFP) was detected using an excitation wavelength of 430 nm and an emission wavelength of 480 nm. For adenylate kinase (AK), enzymatic activity was detected via

an enzymatic cascade (AK Activity Assay Kit, Abcam, Cambridge, UK). AK fluorescence was detected using an excitation wavelength of 535 nm and an emission wavelength of 587 nm.

Microfluidic Device Fabrication: Fabrication of the microlens/channel/micromirror sandwich structure involves six processing steps as shown in Figure S5 (Supporting Information). In the first step, a master mold (consisting of curved structures and rectangular microfluidic channels) was fabricated using a commercially available femtosecond laser lithography system (Photonic Professional GT, Nanoscribe GmbH, Eggenstein-Leopoldshafen, Germany). Polydimethylsiloxane (PDMS) microfluidic devices were then cast from this master mold using standard soft-lithographic methods. Third, a reflective coating was deposited onto the curved walls using a metal-evaporation process.[22] Such curved structures form compound micromirrors integrated within the microfluidic channels. After bonding of the PDMS device to one side of a glass coverslip, a microlens array was fabricated on the opposite side of the cover glass, again using two-photon lithography.

Microlenses were designed and optimized using the Ray Tracing module provided by COMSOL Multiphysics 5.5 (COMSOL, Burlington, USA). Subsequently, the design was exported and converted into a stereolithographic file format. Micromirrors integrated within the microchannels were fabricated via two-photon lithography using the Photonic Professional GT femtosecond laser lithography system. In the printing process the laser is used to expose a negative resin (IP-S, Nanoscribe, Eggenstein-Leopoldshafen, Germany) by means of a high-numerical aperture objective in a layer-by-layer fashion. The material solidifies only in the region of the laser focus allowing the additive build up nearly arbitrary 3D structures having sub-micron features. Slicing and hatching distances were set to 0.2 and 0.3 µm, respectively. Subsequently, a 10:1 mixture of PDMS monomer and curing agent (Sylgard 184, Dow Corning, Midland, USA) was poured over the master-mold, polymerized at 70 °C for 4 h and then peeled off. A mirror structure containing gold and silver double layers (with thickness of 100 and 150 nm) on the curved surfaces was fabricated via electron-beam evaporation. The coating procedure is identical to a process described elsewhere.[22] The coating on the PDMS surface was removed using Scotch tape, inlet and outlet ports punched using a hole-puncher (Technical Innovations, West Palm Beach, USA) and the structured PDMS substrate bonded to the glass substrate after treating both surfaces in an oxygen plasma (EMITECH K1000X, Quorum Technologies, East Sussex, UK) for 60 s. Subsequently, the microfluidic device was installed into the 3D printer. After manual alignment under the microscope inside the printer, microlenses were printed coaxially to the micromirrors. The microfluidic devices incorporated a straight channel with one inlet and outlet, and a flow-focusing geometry able to form droplets with a width of 20 µm and a height of 30 µm.

Microlenses on the glass coverslip were fabricated from a high optical quality negative photoresist (IP-S, Nanoscribe GmbH, Eggenstein-Leopoldshafen, Germany), whilst wall layers inside the channel were made from a bespoke negative photoresist (an 87:10:3 mixture of trimethylolpropane ethoxylate triacrylate, pentaerythritol triacrylate and Irgacure 369). The lenses were fabricated as a linear array spanning the entire length (4.8 mm) of a 160 µm thin glass cover slip (Menzel-Glaser, Braunschweig, Germany). SEM images were taken to observe the surface morphology of the micro lenses.

Device Operation: The microfluidic device (Figure S3, Supporting Information) integrating a standard flow-focusing nozzle geometry was rendered hydrophobic by treatment with Aquapel (Pittsburgh Glass Works, Pittsburgh, USA). Such a treatment prevented droplet wetting on the microfluidic channel surfaces. Droplet size and generation frequency were regulated via control of the volumetric flow rate of the aqueous and oil streams. Specifically, volumetric flow rates were controlled using a pressure pump OB1 MK2 (Elvesys, Paris, France). Reservoirs were connected to the microfluidic device using a syringe needle (GONANO Dosiertechnik GmbH, Greven, Germany) and Tygon tubing with an inner diameter of 200 µm and an outer diameter of 760 µm (Adtech, Fisher Scientific, Switzerland). The continuous phase comprised a Hydrofluoroether (HFE) 7500 (3 M, St. Paul, USA) containing a 2% w/w biocompatible EA-surfactant (RainDance Technologies, Lexington, USA), to stabilize droplets against coalescence. Two separate inlets were used for the discrete phase: one for the *E. coli* suspension in 2-(N morpholino) ethanesulfonic acid buffer (0.1 M, pH 6.6), and one for the reaction mixture (2 µL AK Convertor, 2 µL AK Developer , 2 µL ADP Substrate, 0.3 µL AK Probe, and 18.7 µL lysis buffer). For initial microfluidic experiments, pressure values were set at 200 mBar for both aqueous phases, and 160 mBar for the oil phase. This led to the production of 28 µm diameter droplets at a frequency of ≈300 Hz. Droplets generated from the flow-focusing nozzles were collected into Eppendorf tubes and incubated off-chip at 20 °C for 60 min. The droplets were reinjected into the optofluidic-detection device using a pressure pump at a pressure of 200 mBar.

Imaging of the Droplets: The microfluidic device was placed on a motorized *x*–*y* translation stage (Mad City Laboratories, Maddison, USA) mounted on an inverted microscope (Nikon Ti-E Microscope, Zurich, Switzerland). Droplets were imaged during experiment using a high-speed camera (µeye, IDS Imaging Development Systems GmbH, Obersulm, Germany) at a frame rate of 1000 frames per second in bright-field mode and with a magnification of 10 × or 20 × . For fluorescence measurements, a 2 × magnification, 0.06 NA Plan Fluor objective lens (Nikon, Zurich, Switzerland) was used. A high-power LED light source operating at 488 nm (SPECTRA X light engine, Lumencor, Beaverton, USA) was used for excitation. The beam was reflected by a dichroic mirror (ZT 488/Chroma AHF, Tübingen, Germany) and focused into the microfluidic device through a Plan Fluor 2 × , NA 0.06, (Nikon, Zurich, Switzerland) objective. For calibration experiments, microdroplets were filled with 10×10^{-6} M fluorescein in 50×10^{-3} M phosphate buffer (pH 8.3). Fluorescence emission originating from individual droplets was collected by the same objective, passed through an emission filter (520/25, Chroma AHF, Tübingen, Germany) and detected with a CMOS camera (Andor Zyla sCMOS, Oxford Instruments, Oxford, UK).

Supporting Information

Supporting Information is available from the Wiley Online Library or from the author.

Acknowledgements

The authors would like to acknowledge support from the Swiss National Science Foundation: Nr. 205321_179055 (P.A.) and ETH Zürich. X.B.C. is a recipient of a Chinese Scholarship Council Ph.D. Fellowship.

Conflict of Interest

The authors declare no conflict of interest.

Keywords

droplets, fluorescence, microfluidics, optics, single-cell

Received: December 31, 2019
Revised: February 21, 2020
Published online: April 20, 2020

[1] T. Thorsen, R. W. Roberts, F. H. Arnold, S. R. Quake, *Phys. Rev. Lett.* **2001**, *86*, 4163.
[2] R. L. Burns, E. P. Duliba, *J. Surfactants Deterg.* **2000**, *3*, 361.

[3] O. J. Dressler, X. C. i. Solvas, A. J. deMello, *Annu. Rev. Anal. Chem.* **2017**, *10*, 1.
[4] F. Lan, J. R. Haliburton, A. Yuan, A. R. Abate, *Nat. Commun.* **2016**, *7*, 11784.
[5] X. Leng, W. Zhang, C. Wang, L. Cui, C. J. Yang, *Lab Chip* **2010**, *10*, 2841.
[6] M. Maeki, H. Yamaguchi, M. Tokeshi, M. Miyazaki, *Anal. Sci.* **2016**, *32*, 3.
[7] M. T. Guo, A. Rotem, J. A. Heyman, D. A. Weitz, *Lab Chip* **2012**, *12*, 2146.
[8] C. Heinis, *Nat. Chem. Biol.* **2014**, *10*, 696.
[9] R. Novak, Y. Zeng, J. Shuga, G. Venugopalan, D. A. Fletcher, M. T. Smith, R. A. Mathies, *Angew. Chem., Int. Ed.* **2011**, *50*, 390.
[10] A. Dufour, V. Shinin, S. Tajbakhsh, N. Guillén-Aghion, J.-C. Olivo-Marin, C. Zimmer, *IEEE Trans. Image Process.* **2005**, *14*, 1396.
[11] E. Balleza, J. M. Kim, P. Cluzel, *Nat. Methods* **2018**, *15*, 47.
[12] P. A. Dunn, H. W. Tyrer, *J. Clin. Med.* **1981**, *98*, 374.
[13] B. Egner, J. Frey, W. Brocklesby, *Chem. Commun.* **1997**, 735.
[14] D.-K. Kang, M. M. Ali, K. Zhang, S. S. Huang, E. Peterson, M. A. Digman, E. Gratton, W. Zhao, *Nat. Commun.* **2014**, *5*, 1.
[15] V. R. Yelleswarapu, H.-H. Jeong, S. Yadavali, D. Issadore, *Lab Chip* **2017**, *17*, 1083.
[16] V. Yelleswarapu, J. R. Buser, M. Haber, J. Baron, E. Inapuri, D. Issadore, *Proc. Natl. Acad. Sci. USA* **2019**, *116*, 4489.
[17] M. Kim, M. Pan, Y. Gai, S. Pang, C. Han, C. Yang, S. K. Tang, *Lab Chip* **2015**, *15*, 1417.
[18] E. Schonbrun, A. R. Abate, P. E. Steinvurzel, D. A. Weitz, K. B. Crozier, *Lab Chip* **2010**, *10*, 852.
[19] J. T. Negou, L. A. Avila, X. Li, T. M. Hagos, C. J. Easley, *Anal. Chem.* **2017**, *89*, 6153.
[20] J. J. Schwartz, S. Stavrakis, S. R. Quake, *Nat. Nanotechnol.* **2010**, *5*, 127.
[21] J. Vila-Planas, E. Fernández-Rosas, B. Ibarlucea, S. Demming, C. Nogués, J. A. Plaza, C. Domínguez, S. Büttgenbach, A. Llobera, *Nat. Protoc.* **2011**, *6*, 1642.
[22] J. Lim, P. Gruner, M. Konrad, J.-C. Baret, *Lab Chip* **2013**, *13*, 1472.
[23] D. Wu, L.-G. Niu, S.-Z. Wu, J. Xu, K. Midorikawa, K. Sugioka, *Lab Chip* **2015**, *15*, 1515.
[24] H. Yang, M. Cornaglia, M. A. M. Gijs, *Nano Lett.*. **2015**, *15*, 1730.
[25] R. Galland, G. Grenci, A. Aravind, V. Viasnoff, V. Studer, J.-B. Sibarita, *Nat. Methods* **2015**, *12*, 641.
[26] S. Zhu, L. Ma, S. Wang, C. Chen, W. Zhang, L. Yang, W. Hang, J. P. Nolan, L. Wu, X. Yan, *ACS Nano* **2014**, *8*, 10998.
[27] N.-T. Nguyen, *Biomicrofluidics* **2010**, *4*, 031501.
[28] H. Yabu, M. Shimomura, *Langmuir* **2005**, *21*, 1709.
[29] E. Schonbrun, S. S. Gorthi, D. Schaak, *Lab Chip* **2012**, *12*, 268.
[30] M.-H. Wu, G. M. Whitesides, *J. Micromech. Microeng.* **2002**, *12*, 747.
[31] N. Ong, Y. Koh, Y. Q. Fu, *Microelectron. Eng.* **2002**, *60*, 365.
[32] J. Albero, L. Nieradko, C. Gorecki, H. Ottevaere, V. Gomez, H. Thienpont, J. Pietarinen, B. Päivänranta, N. Passilly, *Opt. Express* **2009**, *17*, 6283.
[33] M. V. Kunnavakkam, F. M. Houlihan, M. Schlax, J. A. Liddle, P. Kolodner, O. Nalamasu, J. A. Rogers, *Appl. Phys. Lett.* **2003**, *82*, 1152.
[34] Y. Fan, Y. Wu, Y. Chen, Y. C. Kung, T. Wu, K. Huang, H. J. Sheen, P. Y. Chiou, *Biomicrofluidics* **2013**, *7*, 044121.
[35] T. Gissibl, S. Thiele, A. Herkommer, H. Giessen, *Nat. Photonics* **2016**, *10*, 554.
[36] S. Thiele, K. Arzenbacher, T. Gissibl, H. Giessen, A. M. Herkommer, *Sci. Adv.* **2017**, *3*, 1602655.
[37] Z. He, Y.-H. Lee, D. Chanda, S.-T. Wu, *Opt. Express* **2018**, *26*, 21184.